RSC Advances

PAPER

View Article Online
View Journal | View Issue

Cite this: *RSC Adv.*, 2017, **7**, 52192

Superhard B_2CO phases derived from carbon allotropes†

Chao Liu,[a] Mingwei Chen,[b] Julong He,[c] Shuangshuang Yu[a] and Tongxiang Liang*[a]

Received 22nd August 2017
Accepted 4th November 2017

DOI: 10.1039/c7ra09277f

rsc.li/rsc-advances

Two new orthorhombic B_2CO structures (*o*P16- and *o*C16-B_2CO) have been predicted theoretically by manual construction. The calculations of independent elastic constants and phonon dispersion spectra have confirmed the mechanical and dynamical stabilities of *o*P16- and *o*C16-B_2CO at zero pressure. Their formation enthalpies are both negative and lower than several B_2C_XO (X = 1, 2, 3, 5) phases, suggesting they are thermodynamically stable. Based on first-principles calculations, *o*P16- and *o*C16-B_2CO are both superhard materials with indirect band gaps. With excellent hardness and tunable band gaps, B_2CO will attract extensive attention for industrial applications and scientific research.

1. Introduction

Since B–C–O system compounds have been synthesized with compositions $B_6C_{1.1}O_{0.33}$ to $B_6C_{1.28}O_{0.31}$ (ref. 1 and 2) and $B(C,O)_{0.155}$ (ref. 3) experimentally, great attention has been attracted towards designing superhard materials using B–C–O compounds due to strong sp^3 B–O/C covalent bonds.[4–7] Li *et al.* studied B_2CO compounds, which are considered as the simplest ternary B–C–O compounds and are isoelectronic with diamond, and then proposed two new structures, *t*P4 (*t*P4-B_2CO) and *t*I16 (*t*I16-B_2CO), as superhard materials.[4] In Li's opinion, B_2CO tends to be stable in the form of tetragonal structures with strong sp^3 covalent B–C and B–O bonds. Inspired by Li's report, B–C–O system compounds have attracted considerable attention in recent years. Zhang *et al.* studied B_2C_XO compounds and predicted three superhard B_2C_XO ($X \geq 2$) phases: $I4_1/amd$-B_2C_2O, $I\bar{4}m2$-B_2C_3O and $P\bar{4}m2$-B_2C_5O.[5] During their research, a reasonable relation between the carbon content and mechanical behavior of B_2C_XO was established and it was suggested that elastic moduli and hardness will benefit from the high carbon content. In 2016, Wang *et al.* explored the B–C–O system in a pressure range of 0–50 GPa, and proposed a new superhard phase, B_4CO_4, which is metastable under ambient conditions, but thermodynamically stable at high pressures above 23 GPa.[6] However all superhard B–C–O phases belong to the tetragonal crystal system.[4–6] Our previous work reveals that there exist some other superhard B–C–O phases with non-tetragonal crystal system, as *o*P8-B_2CO.[7] Actually, 2-dimensional B–C–O materials have also been studied and proposed as a promising 2-dimensional electronic device materials with tunable band gaps and high carrier mobility.[8]

Carbon, which is widely used in industrial applications and scientific research, has numerous allotropes with abundant properties. Considering that B can combine O/C with strong covalent bonds in solid matter as B–O compounds,[9–12] and B–C compounds.[13–15] Inspired by that *t*P4-, and *t*I16-B_2CO are both diamond-like structures,[4] *o*P8-B_2CO is a lonsdaleite-like structure,[7] even the B_2C_XO ($X \geq 2$) phases are also diamond-like structures and can be derived from different *t*P4-B_2CO supercells with partial B and O replacing by C.[5] Hence, we are curious about that whether the fabricated B–C–O compounds with replacement of partial C atoms by B and O atoms in carbon allotropes are stable and what properties do they possess.

In this paper, we carried out the work with the simplest ternary B–C–O compounds B_2CO as a typical example. Numerous new phases of B_2CO have been constructed manually. Undergo rigorous structural stability analysis including mechanical and dynamical stabilities, two orthorhombic phases were discovered. The formation enthalpies were calculated to demonstrate their thermodynamic stabilities. Based on density function theory (DFT), the mechanical and electronic properties of newly discovered phases have been systematically studied.

2. Computational methods and details

Although evolutionary simulation methods like CALYPSO[16–18] and USPEX[19–21] have been played a significant role in successfully predicting superhard materials[4–7,22,23] all potential crystal structures studied here were constructed manually. Here we conceived and constructed new structures following the steps below: (a) extensively selected carbon allotropes with strong sp^3

[a]School of Materials Science and Engineering, Jiangxi University of Science and Technology, Ganzhou 341000, China. E-mail: liang_tx@126.com
[b]Institute of Engineering Research, Jiangxi University of Science and Technology, Ganzhou 341000, China
[c]State Key Laboratory of Metastable Materials Science and Technology, Yanshan University, Qinhuangdao 066004, China

† Electronic supplementary information (ESI) available. See DOI: 10.1039/c7ra09277f

C–C covalent bonds; (b) if the original structure contained $4n$ (n represents integer) atoms, skip step (b), otherwise constructed supercell to make sure the supercell contains $4n$ atoms; (c) broken symmetry and replaced a quarter of C atoms by O atoms, and a half of C atoms by B atoms. C and O atoms are separated by B atoms; (d) found and imposed symmetry.

The underlying geometry optimizations were performed in CASTEP code[24] using DFT. The exchange-correlation functional was adopted CA-PZ form of the local density approximation.[25,26] The another typically functional PBE of generalized gradient approximation was performed.[27] To compare two different algorithms, the calculated results were listed in the ESI.† To ensure the convergence accuracy less than 1 meV, the norm conserving pseudopotential was adopted at a plane wave cutoff kinetic energy of 960 eV and Monkhorst–Pack K points were generated by utilizing $2\pi \times 0.04$ Å^{-1} as K-points separation.[28] During the geometry optimizations *via* BFGS method,[29] iterations were continued until energy change per atom was less than 5×10^{-6} eV; force tensor on atoms was reduced to 0.01 eV Å^{-1}; displacement on atom didn't exceed 5×10^{-4} Å and stress no more than 0.02 GPa. The phonon calculation was implemented in CASTEP *via* the linear response method[30,31] and the elastic constants were calculated by employing the efficient stress–strain method with 9 distorted structures generated for each strain pattern and maximum distortion 0.003. The conventional cells were adopted within the entire research, and the symmetry points for the Brillouin zone are G (0, 0, 0); Z (0, 0, 0.5); T (−0.5, 0, 0.5); Y (−0.5, 0, 0); S (−0.5, 0.5, 0); X (0, 0.5, 0); and R (−0.5, 0.5, 0.5).

3. Results and discussion

Two newly discovered B_2CO structures have been proposed and their crystal structures schematic at zero pressure are shown in Fig. 1. Both of them are orthorhombic system and have 16 atoms per conventional cell. The first, denoted as *o*P16-B_2CO, is a primitive centered structure with space group *Pbam*, and another, denoted as *o*C16-B_2CO, is a *C*-centered (0.5, 0.5, 0) structure with space group *Cmmm*. All coordination numbers of the atoms in *o*P16 and *o*C16 phases are 4, and there are only sp^3 hybridization B–C/O covalent bonds in *o*P16-, and *o*C16-B_2CO.

As depicted in Fig. 1a, *o*P16-B_2CO has a crystal structure similar to Cco-C8 (when B and O are replaced by C, *o*P16-B_2CO change its symmetry to *Cmmm* and form Cco-C8),[32] and the structure is symmetric about the plane $c = 0.5$. Different with Cco-C8, *o*P16-B_2CO has no bonds rigid parallel to c axis. *o*C16-B_2CO, displayed in Fig. 1b, has more higher symmetry than *o*P16-B_2CO. The structure is symmetric about (0.5, 0.5, 0.5), and constructed from Bct-C4.[33] In the *ab* plane, *o*C16-B_2CO can be viewed as the structural units (Fig. 1b, remarked by red line) connected by B–C bonds with 1.596 Å. Also, all the structural units can be viewed as the middle one slipping alone the directions marked by black lines at a given distance 4.443 Å. Once B and O atoms in the structural units are replaced by C atoms, Bct-C4 appeared. In Bct-C4, four neighbour C atoms in the plane $c = 0/0.5$ formed a square. However, in *o*C16-B_2CO, the neighbour 2B and 2O atoms in the plane $c = 0.5$ formed a rhombus with length 1.631 Å and angles ⟨87.17°, 92.83°⟩; the

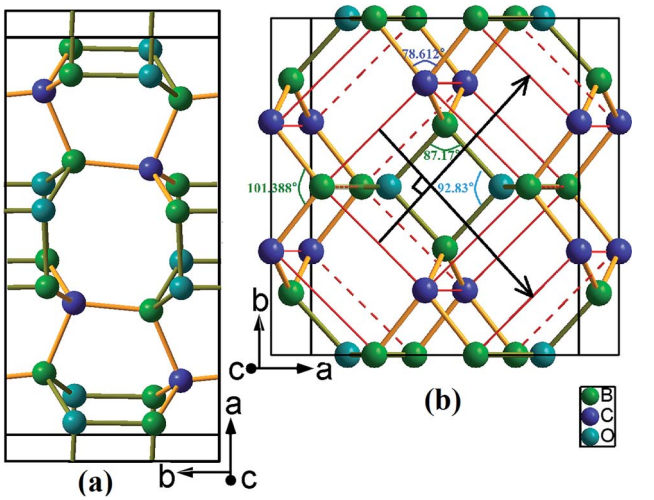

Fig. 1 Structure graphs for (a) *o*P16-, and (b) *o*C16-B_2CO. The sticks in colour dark yellow and light orange represent the bonds B–O and B–C, respectively.

neighbour 2B and 2C atoms in the plane $c = 0$ formed a rhombus with length 1.596 Å and angles ⟨78.612°, 101.388°⟩. More detailed information for the optimized structures at zero pressure is exhibited in Table 1.

The structural stabilities of *o*P16-, and *o*C16-B_2CO are checked by calculating the independent elastic constants C_{ij}s and the phonon dispersion spectra, as presented in Table 2 and Fig. 2, respectively. For an orthorhombic structure, Born criteria are listed in eqn (1).[34]

$$C_{ii} > 0;\ (i = 1, 4, 5, 6);\ C_{11}C_{22} > C_{12}^2;\ C_{11}C_{22}C_{33} + 2C_{12}C_{13}C_{23} - C_{11}C_{23}^2 - C_{22}C_{13}^2 - C_{33}C_{12}^2 > 0; \quad (1)$$

There is no doubt that from Table 2 the C_{ij}s satisfy the criteria above, indicating *o*P16-, and *o*C16-B_2CO are mechanical stable. And no negative frequency was found, which indicates the dynamical stability of these two new B_2CO structures.

For further experimental synthesis, there is necessity to explore the thermodynamic stability of *o*P16-, and *o*C16-B_2CO. Fig. 3 summarizes the formation enthalpies normalized on a per-atom basis of known B_2C_XO ($X = 1, 2, 3, 5$) compounds. The formation enthalpy (ΔH_f), which with respect to the separate phases, is quantified by eqn (2):

$$\Delta H_f = H_{B_2C_XO} - 2H_B - xH_C - \frac{1}{2}H_{O_2}; \quad (2)$$

where diamond C, α-B[35] and α-O_2 (ref. 36) are selected as the separate phases. For *o*P16-, and *o*C16-B_2CO, both have significant negative enthalpies, demonstrating that they are difficult to dissociate into elemental α-B, α-O_2, and diamond C at zero pressure. Compared to *o*P8-B_2CO, formation enthalpy of *o*P16-B_2CO has 14 meV (ΔH_f) per atom advantage at zero pressure. Even *o*P16-B_2CO has nearly identical formation enthalpy with *t*P4-B_2CO, only 3 meV disparity per atom. Although *o*C16-B_2CO has the highest enthalpy among all five B_2CO structures, its formation enthalpy is only 68 meV per atom higher than that of

Table 1 Space groups (S.G.), lattice parameters *a*, *b*, *c* (Å), ρ (g cm^{-3}) and Atomic Wyckoff Positions (A.W.P) for *o*P16-, and *o*C16-B_2CO

	S.G.	*a*	*b*	*c*	ρ	A.W.P.
*o*P16	*Pbam*	8.847	4.364	2.603	3.280	B1 4*h*(0.824, 0.181, 0.5); B2 4*g*(0.911, 0.694, 0); C 4*h*(0.342, 0.680, 0.5); O 4*g*(0.409, 0.177, 0)
*o*C16	*Cmmm*	6.142	6.421	2.601	3.214	B1 4*j*(0, 0.816, 0.5); B2 4*g*(0.165, 0.5, 0); C 4*i*(0, 0.692, 0); O 4*h*(0.317, 0.5, 0.5)

Table 2 Independent elastic constants C_{ij}, and mechanical property parameters as *B*, *G*, *E*, and μ of *o*P16-, and *o*C16-B_2CO. C_{ij}, *B*, *G*, and *E* are expressed in GPa, and μ is dimensionless unit

	C_{11}	C_{22}	C_{33}	C_{44}	C_{55}	C_{66}	C_{12}	C_{13}	C_{23}	*B*	*G*	*E*	μ
*o*P16	664.6	760.3	757.0	236.0	269.0	244.5	112.7	98.2	72.7	305.2	273.9	632.6	0.155
*o*C16	542.4	619.1	778.1	266.7	214.6	218.5	169.1	61.2	129.9	293.3	241.5	568.4	0.177

o*P*8-B_2CO, and far lower than that of B_2C_xO ($x = 2, 3, 5$) phases (228 meV: $I4_1/amd$-B_2C_2O; 339 meV: $I\bar{4}m2$-B_2C_3O; and 497 meV: $P\bar{4}m2$-B_2C_5O). Hence, *o*P16-, and *o*C16-B_2CO may exist as metastable phases. Both formation enthalpy of *o*P16-, and *o*C16-B_2CO decrease with the pressure increase, which indicate these two new B_2CO may be acquired through the synthesis path with loading pressure.

The third-order Birth–Murnaghan equation of state (EOS) for the pressure (*P*)–volume (*V*) relation of *o*P16-, and *o*C16-B_2CO is adopted to fit the 17 pair *P*–*V* data for these two new B_2CO compounds, as presented in Fig. 4.

$$P(V) = \frac{3}{2}B_0\left[\left(\frac{V}{V_0}\right)^{-\frac{7}{3}} - \left(\frac{V}{V_0}\right)^{-\frac{5}{3}}\right]\left\{1 + \frac{3}{4}(B'_0 - 4) \times \left[\left(\frac{V}{V_0}\right)^{-\frac{2}{3}} - 1\right]\right\} \quad (3)$$

The equilibrium volume (V_0), bulk modulus (B_0) and its first order pressure derivative (B'_0) are obtained from eqn (4) and displayed in insert table in Fig. 4.

When loading with hydrostatic pressure to 80 GPa, both *o*P16-, and *o*C16-B_2CO sustain the volume shrinkage without mutation and share the similar shrinkage rates, 17.15% for *o*P16-B_2CO and 17.60% for *o*C16-B_2CO.

The mechanical property parameters including bulk modulus *B*, shear modulus *G*, Young modulus *E*, and Poisson ratio μ of *o*P16-, and *o*C16-B_2CO are listed in Table 2. *B* and *G* can be acquired by independent elastic parameter, then *E* and μ can be obtained by *B* and *G*.[37] Generally speaking, *B* represents the ability to resist volume deformation by loading pressure, *G* characterizes the ability to resist deformation upon shear stress.[38] Both *o*P16-, and *o*C16-B_2CO have very large *B* (~300 GPa) and *G* (above 240 GPa), indicating the excellent resistance to volume deformation by pressure stress and shear stress.

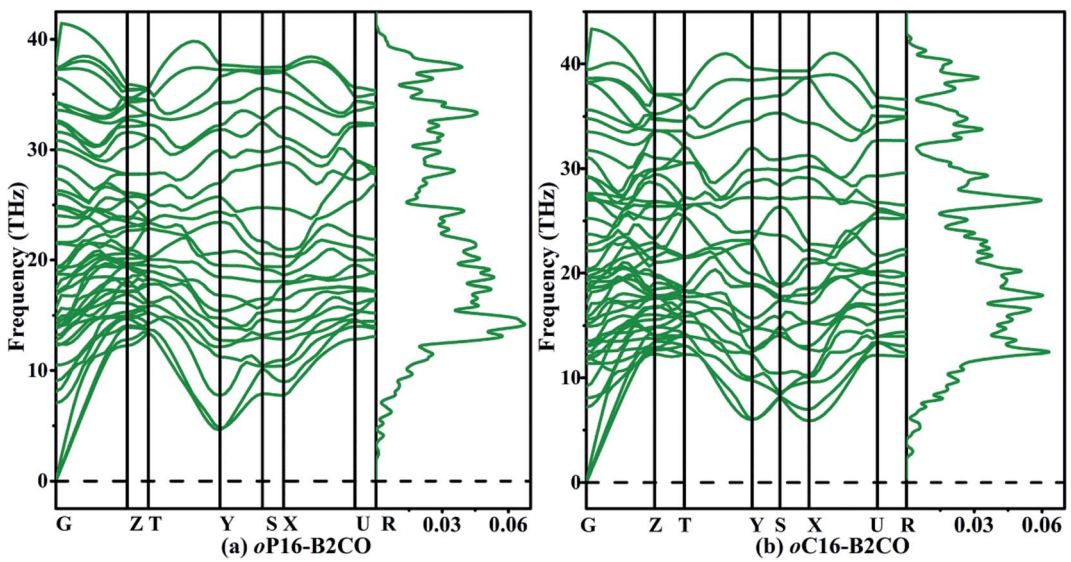

Fig. 2 Phonon dispersion spectra (left panel) and phonon density of states (right panel) of (a) *o*P16-, and (b) *o*C16-B_2CO at zero pressure.

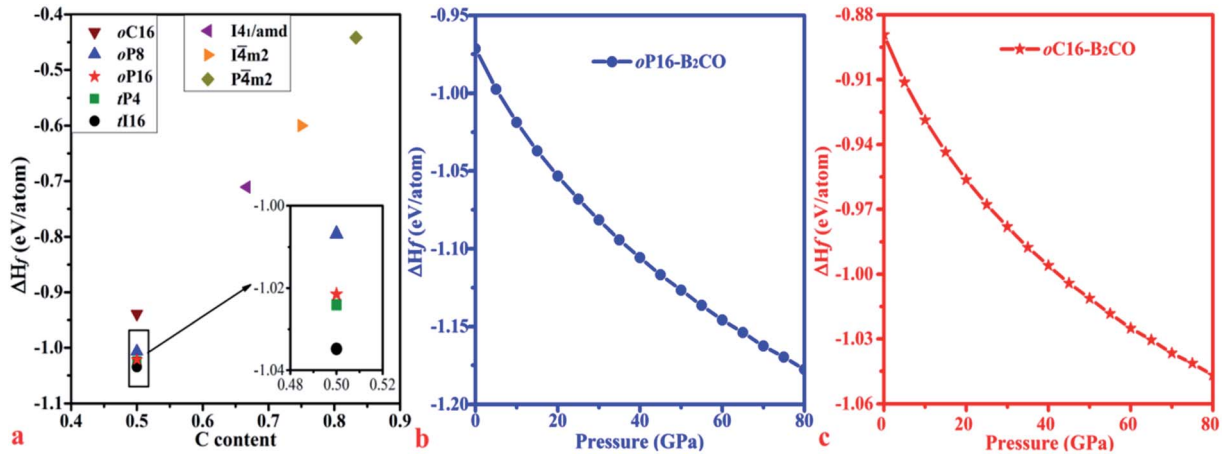

Fig. 3 Calculated formation enthalpies of B_2C_XO phases with different C contents as $x/(1 + x)$ at zero pressure (a) and formation enthalpies of (b) oP16-, and (c) oC16-B_2CO as a function of pressure.

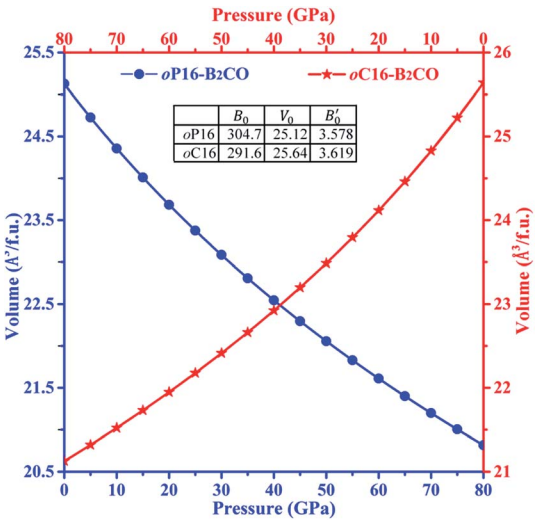

Fig. 4 Volume–pressure relationships for oP16-, and oC16-B_2CO. The geometric patterns and solid lines represent the calculated data and fitting results, respectively.

Elastic anisotropy can give a prediction of the arrangement of the atoms in each direction, the bonding properties, and some chemical characteristics in different directions of materials. An illustrative way of the elastic anisotropy is described by a three-dimensional surface map representation. The curved surface map shows the variation of elastic modulus with crystallographic direction. For orthorhombic crystal, the directional dependence of the Young's modulus is given by eqn (4)[39]

$$E^{-1} = l_1^4 S_{11} + 2l_1^2 l_2^2 S_{12} + 2l_1^2 l_3^2 S_{13} + l_2^4 S_{22} + 2l_2^2 l_3^2 S_{23} + l_3^4 S_{33} + l_2^2 l_3^2 S_{44} + l_1^2 l_3^2 S_{55} + l_1^2 l_2^2 S_{66}; \quad (4)$$

where l_1, l_2 and l_3 are the direction cosines. S_{ij} represents the elastic compliance constants, the inverse of C_{ij}.

Actually, Young's modulus of the three main axis direction satisfy the following relations: $E_{[100]}=1/S_{11}$, $E_{[010]}=1/S_{22}$, $E_{[001]}=1/S_{33}$. For oP16-B_2CO, the b and c axes have the almost consistent Young's modulus (736 GPa and 738 GPa, respectively), which higher that of a axis with 100 GPa. For oC16-B_2CO, Young's modulus for three main axes a, b, and c are 495 GPa, 550 GPa and 750 GPa, the gradually increasing values also illustrated the obvious anisotropy.

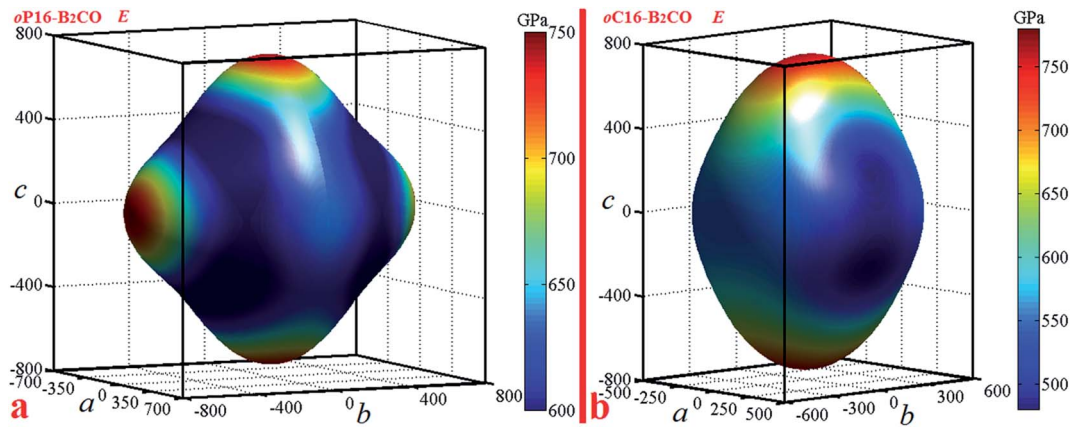

Fig. 5 Directional dependence of the Young's modulus for (a) oP16-, and (b) oC16-B_2CO.

Table 3 Calculated volume V for unit cell (Å^3), bond parameter as bond-type μ, bond length d^{μ} (Å), bond number n^{μ} and H_V (GPa) for *o*P16-, and *o*C16-B_2CO at zero pressure

	V	μ	d^{μ}	n^{μ}	N_e^{μ}	f_i^{μ}	H_V^{μ}	H_V
*o*P16	100.504	B–C(I)	1.541	8	0.612	0.323	58.268	47.817
		B–C(II)	1.582	4	0.565	0.181	61.233	
		B–C(III)	1.588	4	0.559	0.110	65.585	
		B–O(I)	1.596	4	0.709	0.785	33.951	
		B–O(II)	1.621	4	0.676	0.831	29.956	
		B–O(III)	1.623	8	0.673	0.495	44.397	
*o*C16	102.560	B–C(I)	1.524	8	0.619	0.333	59.685	46.222
		B–C(II)	1.596	8	0.539	0.181	58.071	
		B–O(I)	1.602	8	0.685	0.521	45.061	
		B–O(II)	1.631	8	0.649	0.816	29.226	

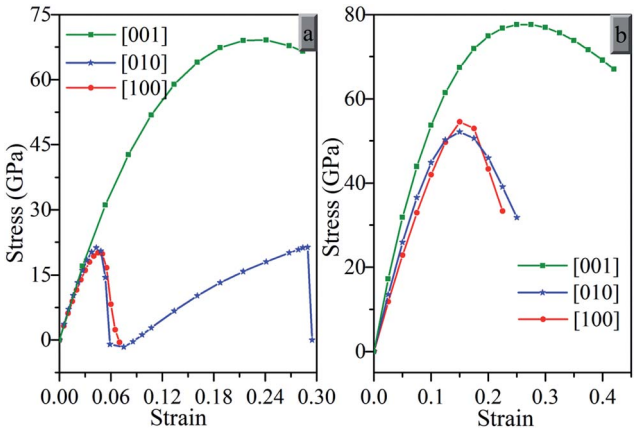

Fig. 6 Calculated tensile stress–strain relations. (a) *o*P16-, and (b) *o*C16-B_2CO.

For an isotropic crystal, the 3D curved surface would exhibit a spherical shape. The deviation degree from the spherical surface indicates the extent of anisotropy (Fig. 5).

As material' fundamental mechanical property, hardness is extensively used and can be theoretically predicted. Here, we calculated the Vickers hardness (H_V) of *o*P16-, and *o*C16-B_2CO by adopting bond resistance model.[40,41]

$$H_V = 350 N_e^{2/3} e^{-1.191 f_i} d^{-2.5} \quad (5)$$

N_e is the electron density; f_i is Phillips iconicity of B–C/O bonds, which can be calculated from eqn (6). d is the bond length. Here we chose 0.75 as P_c value.

$$f_i = [1 - \exp(-|P_c - P|/P)]^{0.735} \quad (6)$$

The calculated hardness of *o*P16-, and *o*C16-B_2CO displayed in Table 3 are both beyond 40 GPa, indicating that the two newly explored B_2CO are superhard materials. The B–C–O system compounds may have potential industrial applications as superhard materials.

A popular approach[42–45] to understand the structural deformation and strength has been extensively applied to solid material under specified strains.[46] It is the material's ideal strength which is defined as the stress at which a perfect crystal changes mechanically unstable, that sets an upper limit for material strength. The atomistic mechanism for structural deformation and failure models can be thorough understanding with the studies of strain–stress relations and bond-breaking processes.

Fig. 6 presents the calculated strain–stress relations for *o*P16-, and *o*C16-B_2CO under tensile strains in three principal symmetry crystallographic directions ([100], [010], and [001]). It can be seen that both *o*P16-, and *o*C16-B_2CO have large stresses with strain exist in the [001] than [010] and [100] directions. Along the [001] direction, *o*P16-B_2CO has a peak tensile stresses 69.1 GPa with a strain of 0.225, and 77.6 GPa with strain 0.275 for *o*C16-B_2CO. The tensile strengths of *o*C16-B_2CO along the [100] and [010] both reach a peak tensile stresses at strain 0.15 with 54.5 GPa and 52.1 GPa, respectively. *o*P16-B_2CO has a peak tensile stress 20.1 GPa with a strain of 0.045. As for the [010] direction of *o*P16-B_2CO, there are two observable peak 21.3 GPa, corresponding these bonds along b axis as B–O bonds breaking

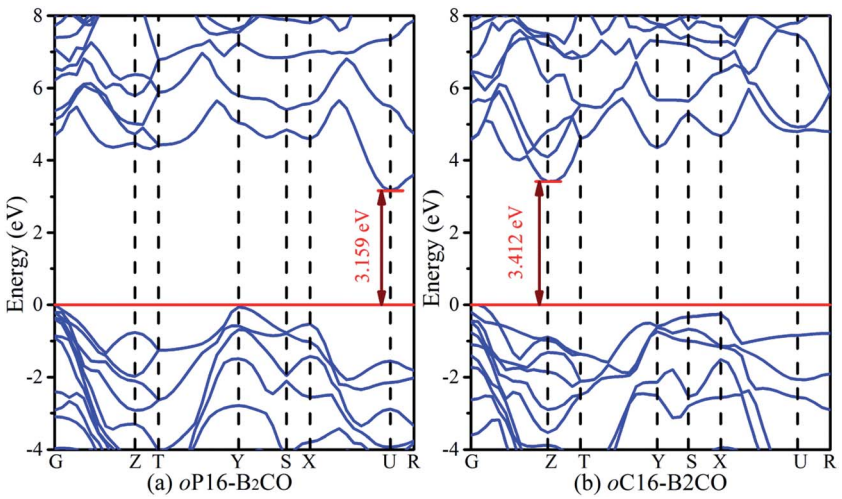

Fig. 7 Calculated electronic band structures for *o*P16-, and *o*C16-B_2CO at zero pressure. The Fermi level is represented by a horizontal red line.

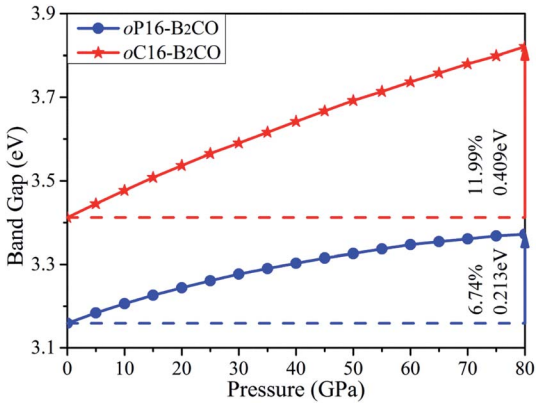

Fig. 8 Calculated band gaps as a function of pressure for *o*P16-, and *o*C16-B_2CO.

with a strain of 0.04 and B–C bonds breaking with a strain of 0.27 respectively. The calculated strain–stress relations reveal anisotropy of *o*P16-, and *o*C16-B_2CO.

The band structures of these superhard B_2CO phases along the symmetry points for the Brillouin zone at zero pressure are calculated and shown in Fig. 7. Both *o*P16-, and *o*C16-B_2CO are semiconductors with indirect band gaps. For *o*P16-B_2CO, the valence band (VB) maximum and conduction band (CB) minimum are located at *G* point and *U* point, respectively, and they are separated by a forbidden band of 3.159 eV. For *o*C16-B_2CO, the VB maximum and CB minimum are located at *G* point and *Z* point, respectively, and separated by a forbidden band of 3.412 eV. For *o*P16-, and *o*C16-B_2CO, the calculated band gaps are 3.159 eV and 3.412 eV, respectively. With the different crystal systems and their atomic stack, these superhard B_2CO (*t*P4-, *t*I16-, and *o*P8-B_2CO within) with the tuneable band gaps from 1.7 eV to 3.5 eV may have potential application in semiconductor industry in future (Fig. 7).

The values of band gaps as a function of pressure in ranges of 0–80 GPa are calculated and plotted in Fig. 8. The band gap of *o*P16-, and *o*C16-B_2CO increases with pressure simultaneously within the whole studied pressure range. For *o*C16-B_2CO, the gap's increase degree is 0.409 eV/11.99%, higher than that of *o*P16-B_2CO (0.213 eV/6.74%).

With the pressure increasing, bonding states and anti-bonding states appear gradually emerges, result in the energy of VB decline and the energy of CB increase, the VB expand to the lower energy region and CB to the higher energy region, the gap increases. The influence on electronic band can be analyzed based on partial specific band morphology under different pressures. Thus the bands with the minimum CB and maximum VB at 0 GPa are selected, and their morphology under different pressure are studied, as Fig. 9. We denoted the difference between maximum and minimum of the selected CB as ΔC, and of VB as ΔV.

For *o*P16-B_2CO with pressure in 0–80 GPa, the minimum energy of CB increase, lead to the gap increases uninterruptedly. The ΔV and ΔC both increase with pressure, indicates the energy range of the selected bands are broaden. It's not just an exception, thus as a whole, the energy range of VB and CB are both broader. The energy of VB is lower, while for CB is higher. The pressure's influence can also be detected based on entire density of states (DOS). As displayed in Fig. 10a, for *o*P16-B_2CO,

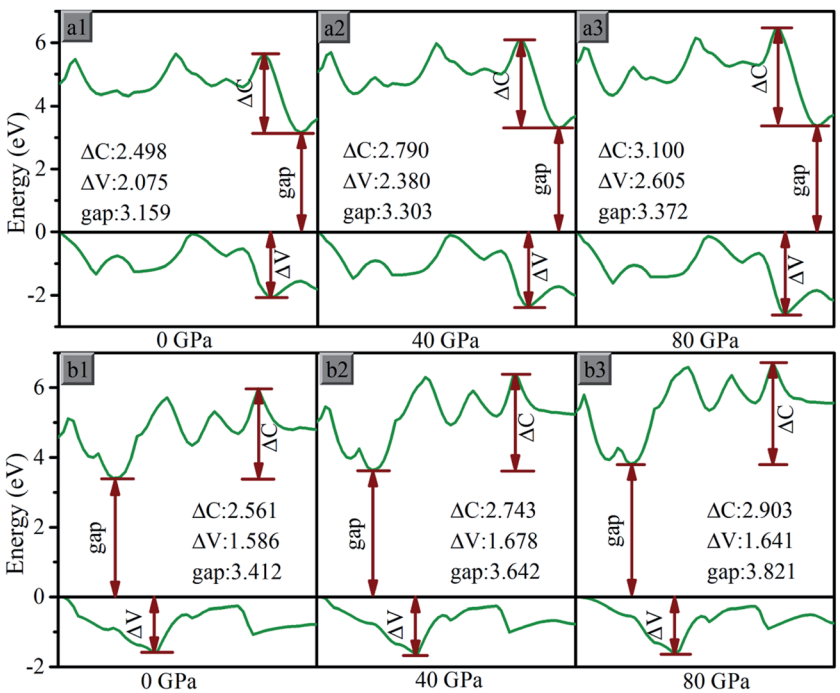

Fig. 9 The maximum value band and minimum conduction band for (a) *o*P16-, and (b) *o*C16-B_2CO at different pressures. The Fermi level is represented by a horizontal black line.

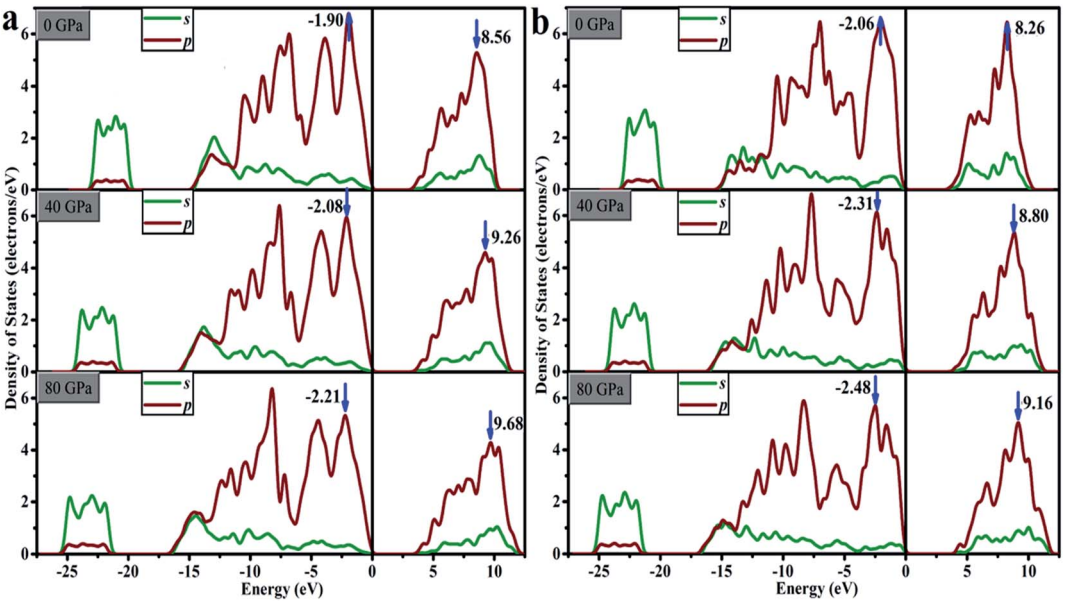

Fig. 10 DOS for (a) *o*P16-, and (b) *o*C16-B_2CO at different pressures.

during the pressure increasing, the energy category of VB (CB) continuously enlarge to the low (high) energy region; the position of the highest peak of VB (CB) has been moved to lower (higher) energy region and the peak height has been reduced.

As for *o*C16-B_2CO, the ΔC increases with pressure, indicates the energy range of the selected bands are broaden, while the ΔV undergoes a process with increase–decrease. As displayed in Fig. 10b, for *o*C16-B_2CO, the energy category of VB (CB) continuously enlarge to the low (high) energy region; the position of the highest peak of VB (CB) has been moved to lower (higher) energy region and the peak height has been reduced.

4. Conclusions

By manual building B_2CO phases from widely known allotropes of carbon, we proposed two new B_2CO (*o*P16-, and *o*C16-B_2CO), derived from Cco-C8 and Bct-C4, respectively. Based on the first-principles study, the elastic constants and phonon dispersion spectra declare that *o*P16-, and *o*C16-B_2CO are mechanically and dynamically stable. Their formation enthalpies, respected to the separate phases, are both negative and lower than that of B_2C_XO ($X = 1, 2, 3, 5$), suggesting thermodynamically stable. *o*P16-B_2CO even has the formation enthalpy which is closed with *t*P4-B_2CO and lower than *o*P8-B_2CO. Based on bond resistance model for hardness prediction, *o*P16-, and *o*C16-B_2CO are both superhard with high hardness values of 47.817 GPa and 46.222 GPa, respectively. Electronic property calculation illustrates that the two newly discovered phases are all semiconductors with indirect band gaps of 3.159 eV and 3.412 eV, respectively. The band gap value as a function of pressure in ranges of 0–100 GPa indicate that pressure has an obvious influence on the band gaps of *o*P16-, and *o*C16-B_2CO. The excellent mechanical and electronic properties indicate the attractive prospect for B–C–O compounds in industrial application and scientific research.

Conflicts of interest

There are no conflicts to declare.

Acknowledgements

This work was supported by the National Science Foundation of China (Grant No. 91326203 and 51421091) and Jiangxi University of Science and Technology Scientific Research Starting Foundation (jxxjbs17053).

References

1 L. A. J. Garvie, H. Hubert, W. T. Petuskey, P. F. McMillan and P. R. Buseck, *J. Solid State Chem.*, 1997, **133**, 365–371.
2 H. Hubert, L. A. Garvie, B. Devouard and P. F. McMillan, *MRS Proceedings*, 1997, **499**, 315–320.
3 N. Bolotina, T. Dyuzheva and N. Bendeliani, *Crystallogr. Rep.*, 2001, **46**, 734–740.
4 Y. Li, Q. Li and Y. Ma, *Europhys. Lett.*, 2011, **95**, 66006.
5 M. Zhang, H. Yan, B. Zheng and Q. Wei, *Sci. Rep.*, 2015, **5**, 15481.
6 S. Wang, A. R. Oganov, G. Qian, Q. Zhu, H. Dong, X. Dong and M. M. D. Esfahani, *Phys. Chem. Chem. Phys.*, 2016, **18**, 1859–1863.
7 C. Liu, Z. Zhao, K. Luo, M. Hu, M. Ma and J. He, *Diamond Relat. Mater.*, 2016, **73**, 87–92.
8 S. Zhou and J. Zhao, *Nanoscale*, 2016, **8**, 8910–8918.
9 T. Endo, T. Sato and M. Shimada, *J. Mater. Sci. Lett.*, 1987, **6**, 683–685.

10 M. Kobayashi, I. Higashi, C. Brodhag and F. Thevenot, *J. Mater. Sci.*, 1993, **28**, 2129–2134.
11 H. Hubert, B. Devouard, L. A. Garvie, M. O'Keeffe, P. R. Buseck, W. T. Petuskey and P. F. McMillan, *Nature*, 1998, **391**, 376–378.
12 H. Dong, A. R. Oganov, Q. Wang, S. N. Wang, Z. Wang, J. Zhang, M. M. Esfahani, X. F. Zhou, F. Wu and Q. Zhu, *Sci. Rep.*, 2016, **6**, 31288.
13 V. L. Solozhenko, O. O. Kurakevych, D. Andrault, Y. Le Godec and M. Mezouar, *Phys. Rev. Lett.*, 2009, **102**, 015506.
14 P. Zinin, L. Ming, H. Ishii, R. Jia, T. Acosta and E. Hellebrand, *J. Appl. Phys.*, 2012, **111**, 114905.
15 M. Chen, J. W. McCauley and K. J. Hemker, *Science*, 2003, **299**, 1563–1566.
16 Y. C. Wang, J. A. Lv, L. Zhu and Y. M. Ma, *Phys. Rev. B: Condens. Matter Mater. Phys.*, 2010, **82**, 094116.
17 Y. C. Wang, J. Lv, L. Zhu and Y. M. Ma, *Comput. Phys. Commun.*, 2012, **183**, 2063–2070.
18 H. Wang, Y. Wang, J. Lv, Q. Li, L. Zhang and Y. Ma, *Comput. Mater. Sci.*, 2016, **112**, 406–415.
19 A. R. Oganov and C. W. Glass, *J. Chem. Phys.*, 2006, **124**, 244704.
20 A. R. Oganov, A. O. Lyakhov and M. Valle, *Acc. Chem. Res.*, 2011, **44**, 227–237.
21 A. O. Lyakhov, A. R. Oganov, H. T. Stokes and Q. Zhu, *Comput. Phys. Commun.*, 2013, **184**, 1172–1182.
22 X. Zhang, Y. Wang, J. Lv, C. Zhu, Q. Li, M. Zhang, Q. Li and Y. Ma, *J. Chem. Phys.*, 2013, **138**, 114101.
23 Q. Yan, B. Wang, Y. X. Wang, J. Yang and G. Yang, *J. Chem. Phys.*, 2014, **140**, 224704.
24 S. J. Clark, M. D. Segall, C. J. Pickard, P. J. Hasnip, M. J. Probert, K. Refson and M. C. Payne, *Z. Kristallogr.*, 2005, **220**, 567–570.
25 J. P. Perdew and A. Zunger, *Phys. Rev. B: Condens. Matter Mater. Phys.*, 1981, **23**, 5048–5079.
26 D. M. Ceperley and B. Alder, *Phys. Rev. Lett.*, 1980, **45**, 566–569.
27 J. P. Perdew, K. Burke and M. Ernzerhof, *Phys. Rev. Lett.*, 1996, **77**, 3865–3868.
28 H. J. Monkhorst and J. D. Pack, *Phys. Rev. B: Condens. Matter Mater. Phys.*, 1976, **13**, 5188–5192.
29 B. G. Pfrommer, M. Côté, S. G. Louie and M. L. Cohen, *J. Comput. Phys.*, 1997, **131**, 233–240.
30 S. Baroni, P. Giannozzi and A. Testa, *Phys. Rev. Lett.*, 1987, **58**, 1861–1864.
31 P. Giannozzi, S. De Gironcoli, P. Pavone and S. Baroni, *Phys. Rev. B: Condens. Matter Mater. Phys.*, 1991, **43**, 7231–7242.
32 Z. Zhao, B. Xu, X. F. Zhou, L. M. Wang, B. Wen, J. He, Z. Liu, H. T. Wang and Y. Tian, *Phys. Rev. Lett.*, 2011, **107**, 215502.
33 X. F. Zhou, G. R. Qian, X. A. Dong, L. X. Zhang, Y. J. Tian and H. T. Wang, *Phys. Rev. B: Condens. Matter Mater. Phys.*, 2010, **82**, 134126.
34 F. Mouhat and F.-X. Coudert, *Phys. Rev. B: Condens. Matter Mater. Phys.*, 2014, **90**, 224104.
35 B. Decker and J. Kasper, *Acta Crystallogr.*, 1959, **12**, 503–506.
36 Y. A. Freiman and H.-J. Jodl, *Phys. Rep.*, 2004, **401**, 1–228.
37 Z. Wu, E. Zhao, H. Xiang, X. Hao, X. Liu and J. Meng, *Phys. Rev. B: Condens. Matter Mater. Phys.*, 2007, **76**, 054115.
38 H. B. Ozisik, K. Colakoglu, E. Deligoz and H. Ozisik, *J. Mol. Model.*, 2012, **18**, 3101–3112.
39 J. F. Nye, *Physical Properties of Crystals: Their Representation by Tensors and Matrices*, Oxford University Press, 1985.
40 F. Gao, J. He, E. Wu, S. Liu, D. Yu, D. Li, S. Zhang and Y. Tian, *Phys. Rev. Lett.*, 2003, **91**, 015502.
41 Y. J. Tian, B. Xu and Z. S. Zhao, *Int. J. Refract. Met. Hard Mater.*, 2012, **33**, 93–106.
42 D. Roundy and C. R. Krenn, *Phys. Rev. Lett.*, 1999, **82**, 2713–2716.
43 D. Roundy, C. R. Krenn, M. L. Cohen and J. W. Morris, *Philos. Mag. A*, 2001, **81**, 1725–1747.
44 B. B. Karki, G. J. Ackland and J. Crain, *J. Phys.: Condens. Matter*, 1997, **9**, 8579–8589.
45 C. R. Krenn, D. Roundy, J. W. Morris Jr and M. L. Cohen, *Mater. Sci. Eng., A*, 2001, **319–321**, 111–114.
46 Y. Zhang, H. Sun and C. Chen, *Phys. Rev. Lett.*, 2005, **94**, 145505.